Journal of Systems Engineering and Electronics
Vol. PP, No. 99, August 2023, pp.1 – 14

Modulated-ISRJ rejection using online dictionary learning for synthetic aperture radar imagery

WEI Shaopeng[1,2], ZHANG Lei[3,*], LU Jingyue[4], and LIU Hongwei[2]

1. College of Oceanography and Space Informatics, China University of Petroleum (East China), Qingdao 266580, China; 2. School of Electronics Engineering, Xidian University, Xi'an 710071, China; 3. School of Electronics and Communication Engineering, Shenzhen Campus of Sun Yat-sen University, Guangzhou 518107, China; 4. School of Computer Science and Technology, Xidian University, Xi'an 710071, China

Abstract: In electromagnetic countermeasures circumstances, synthetic aperture radar (SAR) imagery usually suffers from severe quality degradation from modulated interrupt sampling repeater jamming (MISRJ), which usually owes considerable coherence with the SAR transmission waveform together with periodical modulation patterns. This paper develops an MISRJ suppression algorithm for SAR imagery with online dictionary learning. In the algorithm, the jamming modulation temporal properties are exploited with extracting and sorting MISRJ slices using fast-time autocorrelation. Online dictionary learning is followed to separate real signals from jamming slices. Under the learned representation, time-varying MISRJs are suppressed effectively. Both simulated and real-measured SAR data are also used to confirm advantages in suppressing time-varying MISRJs over traditional methods.

Keywords: synthetic aperture radar (SAR), modulated interrupt sampling jamming (MISRJ), online dictionary learning.

DOI: 10.23919/JSEE.2023.000076

1. Introduction

Synthetic aperture radar (SAR) is capable of remote mapping, battlefield reconnaissance under the conditions of all-weather and all-time, which has been widely used in military and civil areas [1−5]. However, SAR imagery is usually fragile in the complex electromagnetic countermeasures to endure intense jamming. Modulated interrupt sampling repeater jamming (MISRJ) is efficient and flexible for SAR interference [6−8], which is usually intentionally modulated to keep considerable coherence with the SAR waveform to obtain considerable coherent processing gain on SAR processing. In MISRJ, the transmitter and the receiver usually share a single antenna, and thus the jammer can be reduced. MISRJ jammer segmentally samples the SAR transmitted signal and modulates a slice of a signal segment to transmit with amplified power [9,10] repeatedly. In the additionally modulated repeater jamming, a balance should be made to achieve sufficient process gain from SAR processing, while enough modulation complexity should be induced to prevent SAR processors from recognizing and suppressing the jamming slice efficiently. In conclusion, MISRJ with complex modulation and periodical transmission is usually difficult to suppress in practical SAR applications.

In order to suppress MISRJ in SAR imaging, a number of anti-jamming algorithms have been developed recently. They can be roughly classed into five categories: parameterized signal decomposition, time-frequency domain suppression, adaptive filtering, blind source separation, and sparse recovery algorithm. For the parameterized signal decomposition algorithms [11−14], MISRJ slices are usually modeled as polynomial phase signal components, and the polynomial parameters are estimated using high order ambiguity function (HAF). After reconstruction of the reference signal with the estimated polynomial parameters, jamming slices are directly subtracted from the received SAR signal. These algorithms perform well when MISRJ matches the polynomial phase signal model, while they would fail in dealing with complex modulated MISRJs. In the time-frequency domain suppression methods [15−19], the raw signal is usually firstly transformed into the time-frequency domain using transforms, such as short-time Fourier transform (STFT), fractional Fourier transform (FrFT)

Manuscript received January 30, 2022.
*Corresponding author.
This work was supported by the National Natural Science Foundation of China (61771372; 61771367;62101494), the National Outstanding Youth Science Fund Project (61525105), Shenzhen Science and Technology Program (KQTD20190929172704911), and the Aeronautical Science Foundation of China (2019200M1001).

and empirical mode decomposition (EMD). Jamming slices are expected to detect in the time-frequency space and suppressed with time-frequency trap filters. It is not difficult to understand that, in trap filtering, SAR signal with identical time-frequency distribution is also filtered out. In the adaptive filtering algorithms [20,21], notch filtering is performed in the time-domain using the estimated MISRJ frequency, which usually leads to severe signal loss. For the blind source separation algorithms [22,23], the multiple snapshots of jamming segments are used as multiple measurements, and the blind separation methods like joint approximate diagonalization of eigen matrixes (JADE) and independent component analysis (ICA) are used to separate SAR signal from the jamming. Because multiple stable measurements are needed, blind jamming separation requires the invariance of jamming within an extended period. This requirement is not easy to be satisfied in real SAR jamming circumstances. The last sort is the sparse recovery algorithm [24−27] where a parameterized dictionary corresponding with jamming time-frequency [28−31] properties is trained by exploiting the coherence of MISRJ slices to represent jamming slices in an optimally sparse manner. With the dictionary, MISRJ slices can be extracted and subtracted from the signal. In the training stage, the time invariance property of jamming and the ground truth of the jamming signal are required to ensure the convergence of reconstruction optimization, which is usually difficult to be satisfied in practical SAR applications.

In conclusion, traditional jamming suppression methods generally assume the time-invariant property of interference. Inevitable severe signal loss is usually introduced in jamming suppression of time-varying MISRJs. Considering the MISRJ property of time-varying complex modulation with high interference to signal ratio (ISR), the online dictionary learning (ODL) MISRJ suppression is proposed. Inspired by the SAR jamming suppression methods [32−35], this algorithm exploits the temporal and periodic MISRJ modulation via ODL. The autocorrelation function of jamming slices is explored to extract temporal parameters to sort jamming slices from SAR pulses. ODL is ready to separate pure jamming slices with periodical modulation to generate multiple jamming basis models. Finally, jamming components can be canceled using CLEAN integrated with match filtering (MF-CLEAN) under the jamming models. The main contributions of this work are summarized as follows.

(i) The proposed algorithm can tackle time-varying complex modulated jamming with online dictionary learning. The algorithm learns the complex MISRJ models from received pulses that yield flexible and adaptive jamming suppression, unlike fixed parametrical methods.

(ii) The proposed algorithm achieves optimal signal fidelity in jamming suppression. The online learned-MISRJ models can precisely represent time-varying jamming slices, improving interference canceling and signal preservation.

This paper is organized as follows: the MISRJ signal model is constructed and the properties of MISRJ are analyzed in Section 2. The MISRJ suppression using ODL is described in Section 3. The simulated and real-measured experiments are performed in Section 4. Finally, the main conclusion is discussed in Section 5.

2. Signal model of MISRJ

SAR transmits the wideband signal to obtain high range resolution, and the linear frequency modulation (LFM) signal is commonly used due to its sizeable time-bandwidth product. It has the formation as

$$S(t)=\mathrm{rect}\left(\frac{t}{T_p}\right)\cdot\exp\left[\mathrm{j}2\pi\left(f_c t+\frac{1}{2}\mu t^2\right)\right] \tag{1}$$

where T_p is the pulse width, f_c is the carrier frequency, μ is the chirp rate, and $\mathrm{rect}(t/T_p)$ is the rectangular window function represented as

$$\mathrm{rect}\left(\frac{t}{T_p}\right)=\begin{cases}0, & \left|\dfrac{t}{T_p}\right|>\dfrac{1}{2}\\ 1, & \left|\dfrac{t}{T_p}\right|\leqslant\dfrac{1}{2}\end{cases}. \tag{2}$$

In order to counter the normal imaging function of SAR in radar electronic counter-measures, intentional interference is an effective for niche-targeting jam of radar's probing. Because traditional interrupt sampling repeater jamming (ISRJ) has a fixed time-frequency response corresponding with transmitting signal, it is easily analyzed and suppressed using time-frequency analysis, parameter estimation, and adaptive filtering methods. In this way, MISRJ is recently proposed to produce wideband jamming to affect the SAR imaging and recognition process. Frequently, the generation process of MISRJ is shown in Fig. 1, and the generation process can be roughly summarized as three steps. Firstly, the receiving antenna is turned to receive the transmitting signal of SAR, and the digital signal can be obtained by band-pass filtering, down-converting and analog to digital (A/D) converting. Then, the sampling segment of the transmitting signal is modulated by a preset filter to obtain the modulated interference signal. Finally, this signal is transmitted by digital to analog (D/A) converting, up converting, and frequency shifter. Based on the generation of MISRJ, the signal slice after A/D converting can be represented as

$$S_s(t)=p(t)*S(t) \tag{3}$$

where $*$ is the Cartesian product, and $p(t)$ is the interrupted sampling function represented as

$$p(t)=\mathrm{rect}\left(\frac{t-\tau_c}{T_c}\right) \tag{4}$$

where T_c is the slice width, and τ_c is the time delay of slice signal. Assume that the modulation filter in frequency domain can be represented as $H(f)$, so the MISRJ in time domain can be represented as

$$S_I(t)=\mathrm{IFT}\{H(f)*S_s(f)\} \tag{5}$$

where $S_s(f)$ is the Fourier transform of signal slice $S_s(t)$ and $\mathrm{IFT}\{\cdot\}$ is the inverse Fourier transform. Generally, the purpose of MISRJ is to produce multiple false targets in SAR image, so the time delay operation of modulated interference is always made to obtain several interference segments. In this way, assume that K segments are transmitted in one pulse, and the transmitted MISRJ of jammer can be represented as

$$S_{\mathrm{MISRJ}}(t)=\sum_{k=0}^{K-1}S_I(t-k\cdot T_c). \tag{6}$$

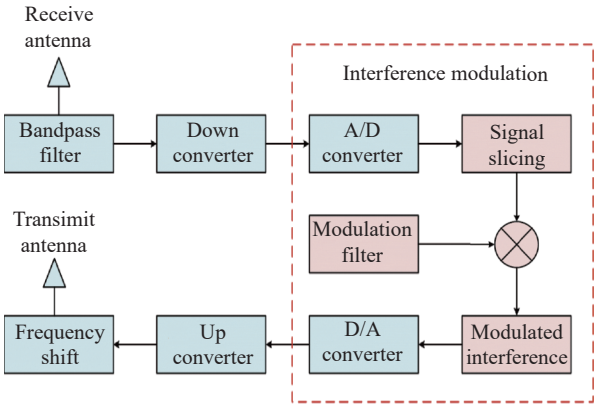

Fig. 1 Generation of MISRJ

Therefore, the SAR echo involved by MISRJ can be represented as

$$S_r(t)=S_0(t)+S_{\mathrm{MISRJ}}(t)+n(t) \tag{7}$$

where $S_0(t)$ is the real SAR echo and $n(t)$ is white Gaussian noise. Analyzing the jamming manner of MISRJ of previous works, the properties of MISRJ can be concluded as three aspects.

(i) Short-time invariance with periodical transmitting mode. MISRJ usually uses single time-sharing transmit-receive antenna, which means that the MISRJ cannot be transmitted when the antenna receives a pulse. Therefore, to increase jamming efficiency and jamming time, the same MISRJ will be periodically transmitted several times once the transmitting signal of SAR is intercepted. In this case, the received jamming of SAR has the property of short-time invariance in several continuous pulses.

(ii) Large power. In order to make an apparent influence on SAR image, the transmitting power is usually considerable. In addition, it is a single trip between jammer and SAR, so the echo power of MISRJ is much larger than the real scene echo power based on the radar power equation.

(iii) Complex modulation manner. Because the modulation process is involved in MISRJ, the jamming is not the strict LFM signal segments and some jamming suppression methods based on ISRJ lose their efficiency. In other words, MISRJ brings about the vast difficulty for SAR anti-jamming. Motivated by these three properties of MISRJ, a kind of interference suppression for SAR imaging based on dictionary learning is proposed and described in the following sections.

3. MISRJ suppression using ODL

Based on the properties of MISRJ, the proposed MISRJ suppression method using ODL for SAR imaging is described in Fig. 2. From Fig. 2, it can be seen that the proposed methods can be divided into three steps: MISRJ segments extraction, ODL for cancellation model generation, and MISRJ suppression.

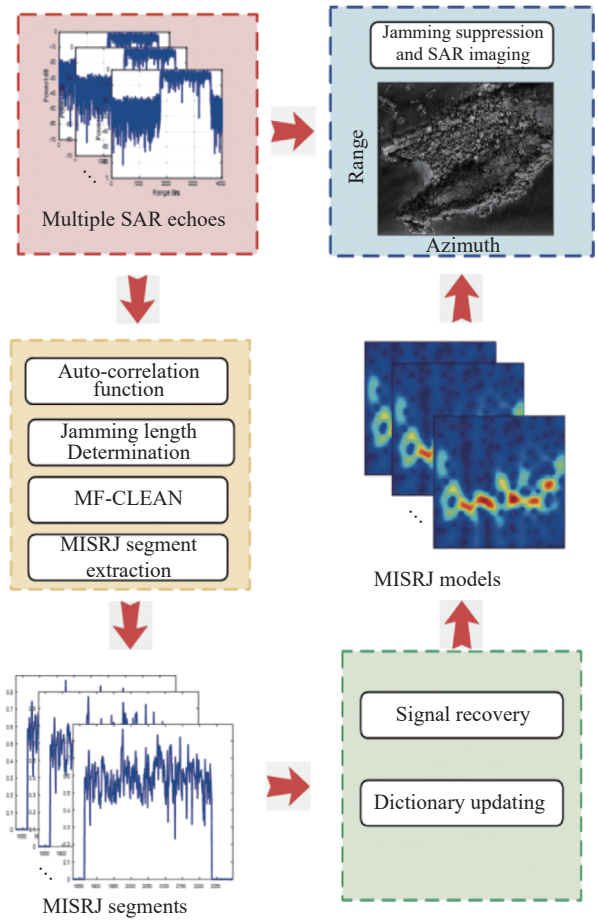

Fig. 2 Flowchart of the proposed method

In this framework, independent MISRJ segments can be extracted using the correlation function. Then, the invari-

ance of MISRJ among different pulses in a short time is utilized, and these similar MISRJ segments can be regarded as generated from one same dictionary and the sparsity can be explored. Because the modulation form and slice position are unknown, dictionary learning can be applied to generate interference models adaptively. Finally, the MISRJ cancellation can be carried out using these models. These three steps are detailed described in the following sections.

3.1 MISRJ segments extraction

First, determine the length of MISRJ. From (7), the auto-correlation function can be calculated as

$$R(\tau)=\sum_{l=1}^{L}S_r(l)*S_r(l-\tau)^*. \tag{8}$$

Because the power of MISRJ is much more higher than the power of the target signal and the jamming to signal ratio (JSR) is usually more than 20 dB, the auto-correlation function mainly reflects the correlation property of MISRJ. In addition, MISRJ segments are the same in one pulse, and there are several peaks in the auto-correlation function. The real-measured SAR echo with MISRJ is shown in Fig. 3. The properties of considerable power and complex modulation can be seen from Fig. 3(a) and Fig. 3(b). Because one SAR pulse includes several serial numbers of MISRJ segments, the length of MISRJ can be calculated from the minimum distance of peak value in the auto-correlation function, as shown in Fig. 3(c).

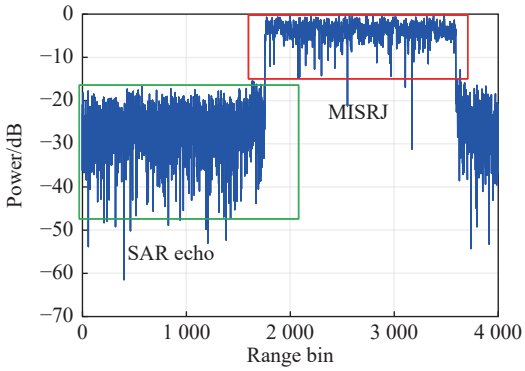

(a) Signal with MISRJ in time domain

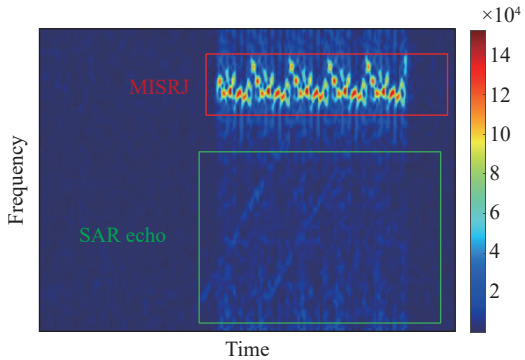

(b) Time frequency distribution of the jamming signal

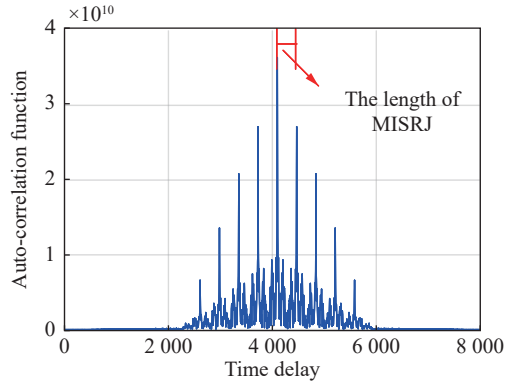

(c) Auto-correlation function of SAR echo

Fig. 3 Real-measured SAR echo with MISRJ

Assume that the position of peak value in the auto-correlation function is $\boldsymbol{P}=[p_1,p_2,\cdots,p_N]$, and the length of MISRJ can be determined by

$$L_{\text{MISRJ}}=\left\lceil\frac{1}{N}\sum_{n=1}^{N}\min\{|p_n-P|\}\right\rceil \tag{9}$$

where $\lceil\cdot\rceil$ is the operation of round up to an integer. Once the length of MISRJ is determined, the segments of MISRJ can be extracted by MF-CLEAN. First, we adopt the sliding window to choose an alternative MISRJ segment searching. Assume that the alternate MISRJ segment in the current sliding window k can be recorded as $S_a^k(t)$, which is used as the reference signal for matched filtering. The output of matched filter can be represented as

$$F_k(t)=S_r(t)\circ S_a^k(-t)^* \tag{10}$$

where $\circ$ is the convolution operation. If this reference signal corresponds with the MISRJ segment, the $F_k(t)$ will have several large peak values equal to the number of MISRJ segments. In other words, if we subtract the reference signal in the peak value position, the rest signal's energy will be significantly decreased, proving that the reference signal is the MISRJ segment. Assume that the position of peak value is in the time of t_p, the rest signal after this CLEAN operation can be represented as

$$\begin{cases}\hat{S}_k(t)=S_r(t)-\exp(\mathrm{j}\varphi)S_a^k(t), & t\in[t_p,t_p+L_{\text{MISRJ}}\cdot T_s]\\ \hat{S}_k(t)=S_r(t), & t\in[0,t_p]\cup[t_p+L_{\text{MISRJ}}\cdot T_s,T_p]\end{cases} \tag{11}$$

where T_s is the sampling time, and φ is the difference of initial phase estimated as

$$\hat{\varphi}=\frac{1}{L_{\text{MISRJ}}}\cdot\sum_{l=0}^{L_{\text{MISRJ}}-1}\frac{S_r(t_p+l\cdot T_s)*S_a^k(t_p+l\cdot T_s)^*}{\left|S_r(t_p+l\cdot T_s)\right|\cdot\left|S_a^k(t_p+l\cdot T_s)\right|}. \tag{12}$$

Due to several MISRJ segments in one pulse, the posi-

tions of the first M peak values are chosen to repeat this CLEAN process and the final rest signal of the k sliding window can be represented as $\tilde{S}_k(t)$, and its rest energy can be represented as

$$E(k)=\sum_{t=0}^{T_p}\tilde{S}_k(t)\cdot\tilde{S}_k(t)^*. \tag{13}$$

In this way, the MISRJ segments can be obtained to choose the reference signal corresponding with low rest energy in one pulse. As metioned above, to increase jamming efficiency and jamming time, the MISRJ periodically transmits the same segments, so we can obtain the MISRJ sets extracted from different pulses, which is denoted as $\boldsymbol{Y}=[S_a^1(t),S_a^2(t),\cdots,S_a^N(t)]$. It should be noted that the signals in this MISRJ set have the same signal structure, and dictionary learning is used to extract this signal structure in the following text.

3.2 ODL for cancellation model generation

In Subsection 3.1, MISRJ segments are extracted from SAR echoes. Based on (7), $\boldsymbol{Y}$ can be denoted as

$$\begin{aligned}\boldsymbol{Y}=&\left[S_r^1(t),S_r^2(t),\cdots,S_r^N(t)\right]+\\&\left[S_{\text{MISRJ}}^1(t),S_{\text{MISRJ}}^2(t),\cdots,S_{\text{MISRJ}}^N(t)\right]+\\&\left[n^1(t),n^2(t),\cdots,n^N(t)\right]=\\&\boldsymbol{S}_r^{1:N}(t)+\boldsymbol{S}_{\text{MISRJ}}^{1:N}(t)+\boldsymbol{N}^{1:N}(t)\end{aligned} \tag{14}$$

where $S_r^k(t)$ is the target echo in the kth extracted MISRJ segments, $S_{\text{MISRJ}}^k(t)$ is the kth MISRJ segment, and $n^k(t)$ is the white Gaussian noise in the kth MISRJ segment. Because MISRJ is invariant in a short time period and the target echo is totally different in different measurement segments, the jamming part of $[S_{\text{MISRJ}}^1(t),S_{\text{MISRJ}}^2(t),\cdots,S_{\text{MISRJ}}^N(t)]$ has a similar jamming signal component. Furthermore, if the principal components of these MISRJ segments can be obtained, these MISRJ segments will be sparsely represented by the linear combination of several independent signal components. Assume that independent signal components can be represented as $\boldsymbol{D}=[d_1,d_2,\cdots,d_M]$, and the MISRJ segments can be derived as

$$\boldsymbol{S}_{\text{MISRJ}}^{1:N}(t)=\boldsymbol{D}\cdot\boldsymbol{X} \tag{15}$$

where $\boldsymbol{X}$ has a dimension of $M\times N$ and sparse property. In this way, the measurements set can be represented as

$$\boldsymbol{Y}=\boldsymbol{D}\cdot\boldsymbol{X}+\boldsymbol{S}_r^{1:N}(t)+\boldsymbol{N}^{1:N}(t)=\boldsymbol{D}\cdot\boldsymbol{X}+\boldsymbol{W}_{sn} \tag{16}$$

where $\boldsymbol{W}_{sn}$ is the signal and noise subspace. Due to the considerable power of MISRJ and sparsity of $\boldsymbol{X}$, we can obtain a pure jamming model using the sparse recovery method as long as $\boldsymbol{D}$ is known. In order to obtain the MISRJ model and separate jamming and signal simultaneously, the problem of generation of the jamming model becomes a joint sparse recovery and dictionary optimal problem. Recently, ODL [36−39] was proposed to realize sparse signal representation in an online way. The ODL method is parameter-free, and it has high solving efficiency and fast convergency advantages compared with traditional dictionary methods. Particularly for large data sizes, this method is significantly faster than other methods and suitable for online processing. This method transforms the problem of joint dictionary learning and sparse recovery to the problem of alternate optimization. In the tth iteration, first, dictionary $\boldsymbol{D}_{t-1}$ obtained by the last iteration is given, and the sparse solution $\boldsymbol{X}_t$ can be calculated by solving a convex optimization problem with one norm constraint, which can be denoted as

$$\boldsymbol{X}_t=\arg\min_{\boldsymbol{X}}\frac{1}{2}\|\boldsymbol{Y}-\boldsymbol{D}_{t-1}\boldsymbol{X}\|_2^2+\lambda\|\boldsymbol{X}\|_1 \tag{17}$$

where λ is the regular factor. Because the cost function in (17) is convex, the convex optimization methods such as conjugate gradient, least absolute shrinkage and selection operator (LASSO), and iterative soft threshold algorithm (ISTA) can be used to obtain this sparse solution. Then, based on the sparse solution $\boldsymbol{X}_t$ in the tth iteration, the dictionary $\boldsymbol{D}_t$ can be updated with the optimization function as

$$\boldsymbol{D}_t=\arg\min_{\boldsymbol{D}}\frac{1}{2}\|\boldsymbol{Y}-\boldsymbol{D}\boldsymbol{X}_t\|_2^2+\lambda\|\boldsymbol{X}_t\|_1. \tag{18}$$

The method of block-coordinate descent with warm restarts can be utilized to update the dictionary. The detailed steps of ODL are summarized in Algorithm 1. Once the dictionary $\boldsymbol{D}$ is obtained, every column vector can be regarded as an MISRJ signal model to eliminate further jamming, described in the following subsection.

Algorithm 1 ODL method

Input: The initial solution $\boldsymbol{X}$, dictionary $\boldsymbol{D}$, regular parameter λ, and measurements jamming $\boldsymbol{Y}$. The maximum iteration number N and auxiliary variables $\boldsymbol{A}_0=0$, $\boldsymbol{B}$=0

Loop n from 1 to N, and in the nth iteration:

Step 1 Find the sparsity solution using LASSO for (17).

Step 2 Update auxiliary variables:

$$\begin{cases}\boldsymbol{A}_n=\boldsymbol{A}_{n-1}+\boldsymbol{X}_{n-1}\boldsymbol{X}_{n-1}^{\mathrm{H}}\\ \boldsymbol{B}_n=\boldsymbol{B}_{n-1}+\boldsymbol{Y}_{n-1}\boldsymbol{X}_{n-1}^{\mathrm{H}}\end{cases}.$$

Step 3 Update dictionary using (19):

$$\begin{cases} u_j = \dfrac{1}{A_n(j,j)}(b_j - \boldsymbol{D}a_j) + d_j \\ d_j = \dfrac{1}{\max\left(\left\|u_j\right\|_2, 1\right)'} u_j \end{cases}$$

where a_j, b_j, and d_j are the jth column of $\boldsymbol{A}_n, \boldsymbol{B}_n$, and $\boldsymbol{D}_{n-1}$, respectively.

Output: $\boldsymbol{D} = \boldsymbol{D}_N, \boldsymbol{X} = \boldsymbol{X}_n$

3.3 MISRJ suppression in SAR echoes

Same as the MISRJ segments extraction in Subsection 3.1, the MF-CLEAN method is used here to suppress jamming and preserve the target signal simultaneously. Assume that the number of M independent signal components is denoted as $\boldsymbol{D}\cdot\boldsymbol{X} = [M_1(t), M_2(t), \cdots, M_M(t)]$, which can be regarded as the independent jamming reference model. First, the matched filter operation is carried out using every model to search the best-matched results and corresponding signal model, which can be derived as

$$M_{\hat{m}}(t) = \arg\max_m \{\max[|S_r(t) \otimes M_m(-t)^*|]\} \tag{19}$$

where $\otimes$ is the Kronecker product, and the position corresponding with the maximum value is p_m. Thus the MISRJ segment in this place can be canceled using the CLEAN method, and the signal after CLEAN can be represented as

$$\begin{cases} \hat{S}(t) = S_r(t) - \exp(\mathrm{j}\varphi) M_m(-t), \ t \in [p_m, p_m + L_{\mathrm{MISRJ}} \cdot T_s] \\ \hat{S}(t) = S_r(t), \ t \in [0, p_m] \cup [p_m + L_{\mathrm{MISRJ}} \cdot T_s, T_p] \end{cases} \tag{20}$$

where T_s is the sampling time, and φ is the difference of initial phase, which can be estimated as

$$\hat{\varphi} = \frac{1}{L_{\mathrm{MISRJ}}} \sum_{l=0}^{L_{\mathrm{MISRJ}}-1} \frac{S_r(t_p + l\cdot T_s) * S_a^k(t_p + l\cdot T_s)^*}{\left|S_r(t_p + l\cdot T_s)\right| \cdot \left|S_a^k(t_p + l\cdot T_s)\right|}. \tag{21}$$

Moreover, we repeat the operation of matched filtering and CLEAN several times until the rest energy decreases. Consequently, the signal after jamming cancellation is obtained. After MISRJ suppression, the SAR imaging can be implemented. The imaging algorithm is widely researched and the imaging methods can be referenced by [1−5].

4. Simulation and real-measured experiments

4.1 Simulation experiment and performance analysis

The simulated data experiments are carried out in this subsection to verify the remarkable performance of the proposed method. The SAR parameters shown in Table 1 simulate the target echoes. In order to simplify the analysis, a point target is set in the scene, and the enemy's jammer intercepts the transmitting signal. After sampling and modulation, the MISRJ is released and received by SAR. For the MISRJ, one segment has a bandwidth of 20 MHz and every received pulse includes four continuous MISRJ segments, and the JSR is set as 30 dB. The SAR echo, the signal after pulse compressing, the signal without jamming after pulse compressing, and the time-frequency distribution of echo are shown in Fig. 4.

Table 1 Simulated SAR parameters

Parameter	Value
f_c/GHz	6
B/MHz	200
T_p/μs	20
F_s/MHz	200
Pulse repetition frequency/Hz	600

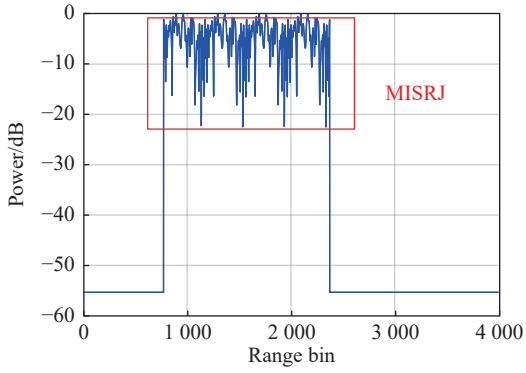

(a) Signal with MISRJ in time domain

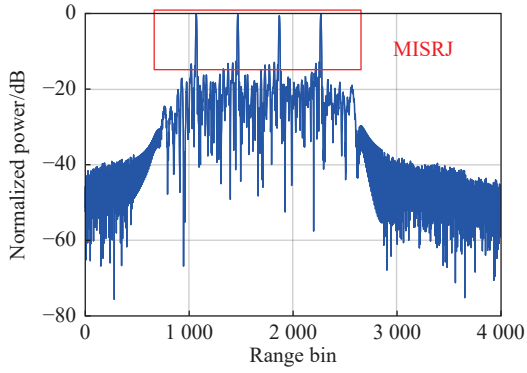

(b) Signal after pulse compressing

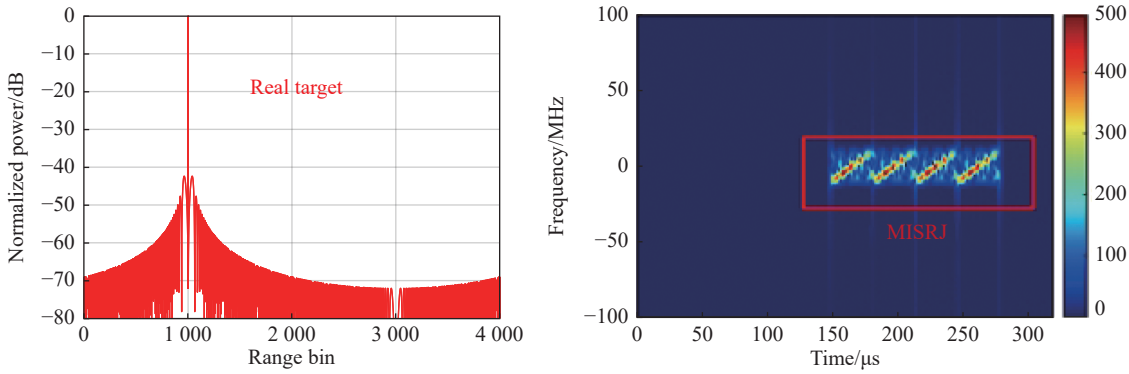

(c) Real target signal after pulse compressing (d) Time-frequency distribution of echo with MTSRJ

Fig. 4 Simulated SAR echo with MISRJ

From Fig. 4(a), it can be seen that the MISRJ segments have more considerable power than the real target echo. In this case, several false targets are formed after pulse compressing shown in Fig. 4(b), and the real target is entirely covered by these false targets shown in Fig. 4(b) and Fig. 4(c). In addition, it can be seen that the MISRJ has complex modulation and its time-frequency distribution has a noticeable difference with the LFM segment. In this way, the MISRJ will have a significantly lousy influence on SAR image.

In order to decrease the influence of MISRJ, we use the proposed MISRJ cancellation with the ODL method to suppress the MISRJ. Firstly, the length of the MISRJ segment is determined as 400 using the correlation function method. Then the MISRJ segments are extracted using the MF-CLEAN method and the MISRJ models are generated using ODL. Finally, the jamming can be canceled using the method described in Subsection 3.3. The results after jamming cancellation are shown in Fig. 5. We can see that the signal with matching filtering of the real target can be correctly output after jamming suppressing, as shown in Fig. 5(a). We enlarge the result of matching filtering and it can be seen that the target power loss after jamming suppressing is low compared with the ideal output of matching filtering. The power loss is 0.205 9 dB in this simulation scene, as shown in Fig. 5(a). In addition, the time-frequency distribution results after jamming suppression are also plotted in Fig. 5(b), and it can be seen that the time-frequency distribution of target appears and the MISRJ can be canceled with little residual jamming. As a comparison, the anti-jamming methods of adaptive filtering [11] and parametric method [20] are used to process the same jamming data. The adaptive filtering and parameterized methods are shown in Fig. 6 and Fig. 7. We can see that the target signal also appears after anti-jamming, but it has more power loss, about 5.196 dB and 2.388 9 dB, and much more residual jamming compared with the proposed method from Fig. 6 and Fig. 7. This simulated experiment verifies that the proposed jamming suppression method has the remarkable performance of canceling jamming and keeping the original target signal.

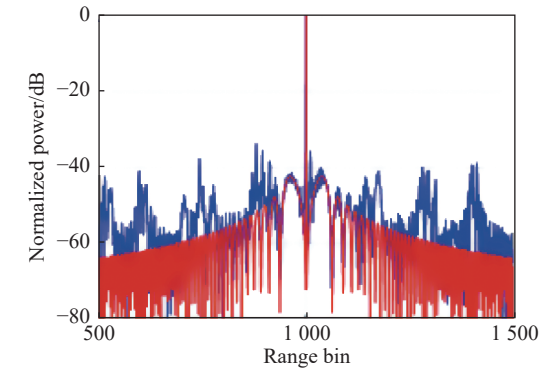

(a) Matched filtering result of jamming echo processed by the proposed method

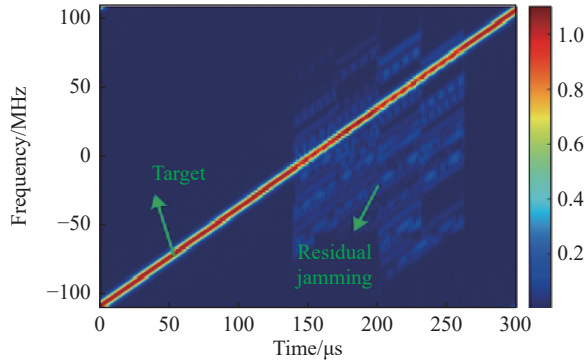

(b)Time-frequency distribution of jamming echo processed by the proposed method

Fig. 5 Anti-jamming results using the proposed method

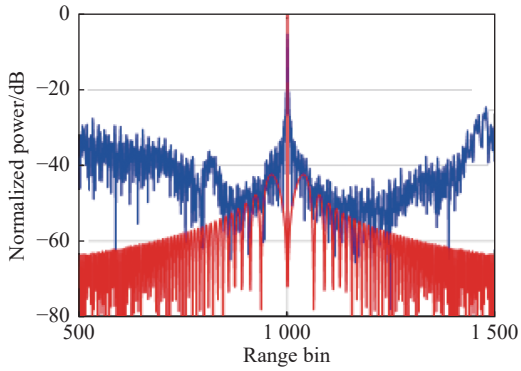

(a) Matched filtering result of jamming echo processed by adaptive filtering method

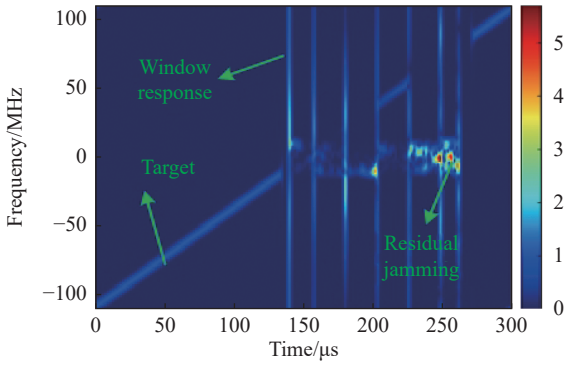

(b) Time-frequency distribution of jamming echo processed by the adaptive filtering method

Fig. 6 Anti-jamming results using the adaptive filtering method

In order to quantitatively analyze jamming suppression performance and real-target signal loss of the proposed method, we use the indexes of residual jamming to signal ratio (RJSR) and power loss (PL) to evaluate them, respectively. RJSR is defined as

$$\mathrm{RJSR}=\frac{\left(\hat{S}(t)-S_r(t)\right)^{\mathrm{H}}\cdot\left(\hat{S}(t)-S_r(t)\right)}{S_r(t)^{\mathrm{H}}\cdot S_r(t)} \tag{22}$$

where $\hat{S}(t)$ is the signal after jamming suppression and $S_r(t)$ is the real-target signal without jamming. $\hat{S}(t)-S_r(t)$ represents the residual jamming signal after jamming suppression. PL can be calculated as

$$\mathrm{PL}=\frac{\max\left\{\left|S_r(t)\otimes s(-t)^*\right|^2\right\}}{\max\left\{\left|\hat{S}(t)\otimes s(-t)^*\right|^2\right\}} \tag{23}$$

where $s(t)$ is the transmitting signal. $\max\left\{\left|S_r(t)\otimes s(-t)^*\right|^2\right\}$ represents the maximum power output of real-target signal without jamming after matching filtering, and $\max\left\{\left|\hat{S}(t)\otimes s(-t)^*\right|^2\right\}$ represents the maximum output of the signal after jamming suppression and matching filtering. In this case, Monte-Carlo experiments with 50 times are carried out to analyze the RJSR and PL in the condition of JSR rarging from 25 dB to 60 dB. The results are shown in Fig. 8 to Fig. 10, and we can see that the proposed method has more petite PL and RJSR, which reveals that the proposed method has less signal loss and jamming residual. It should be noticed that the RJSR decreases with the increase of input JSR because the more extensive the input JSR, the more accurate the jamming model can be obtained, and the better jamming suppression performance can be obtained. On the contrary, because the filtering gain is fixed, the power of residual jamming is increased with the increase of input JSR. In other words, the jamming suppression performance will be degraded in the condition of high input JSR scene.

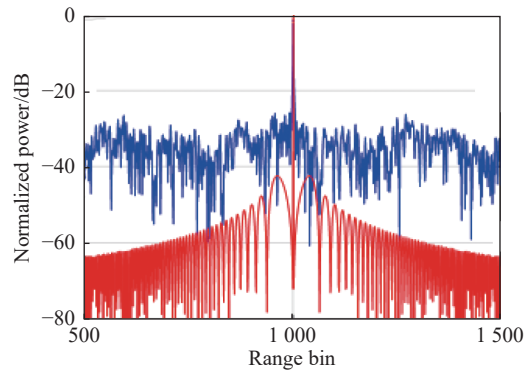

(a) Matched filtering result of jamming echo processed by the parameterized method

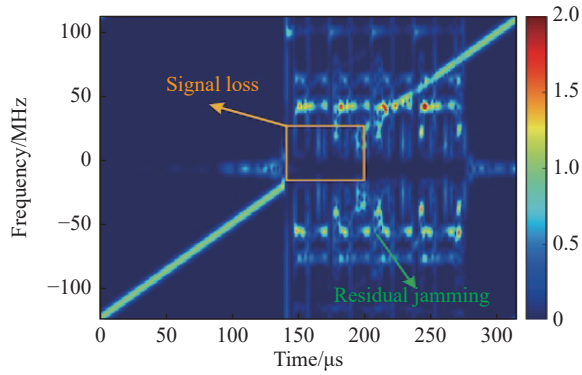

(b) Time-frequency distribution of jamming echo processed by the parameterized method

Fig. 7 Anti-jamming results using the parameterized method

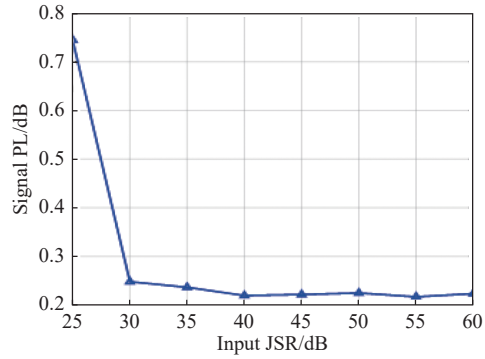

(a) PL with different input JSR using the proposed method

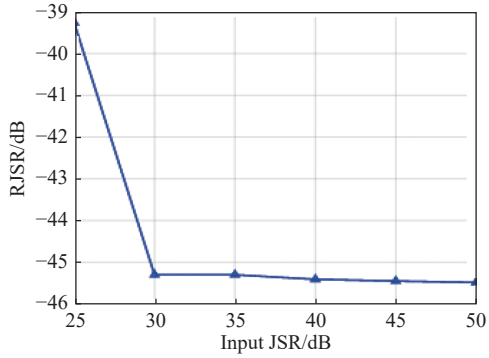

(b) RJSR with different input JSR using the proposed method

Fig. 8 RJSR and PL with different input JSR using the proposed method

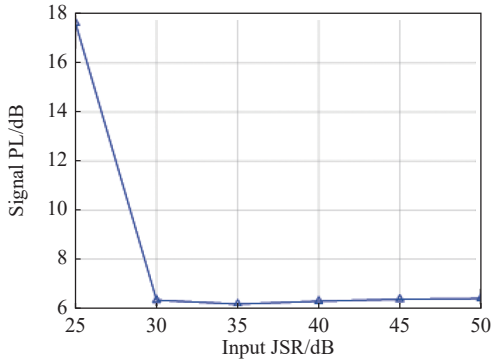

(a) PL with different input JSR using the adaptive filtering method

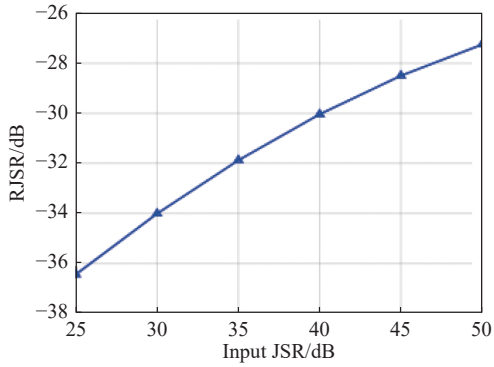

(b) RJSR with different input JSR using the adaptive filtering method

Fig. 9 RJSR and PL with different input JSR using adaptive filtering

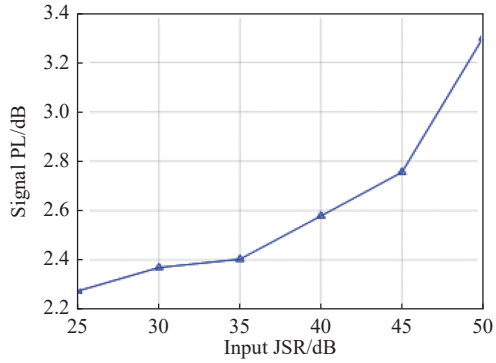

(a) PL with different input JSR using the parameterized method

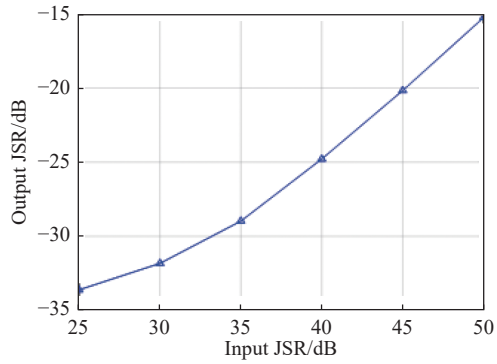

(b) RJSR with different input JSR using the parameterized method

Fig. 10 RJSR and PL with different input JSR using parameterized method

After jamming suppression, a simulated SAR imaging scene is also given to test the SAR imaging performance. The radar parameters are given in Table 1. The simulated scene is shown in Fig. 11(a), and the imaging result without MISRJ is shown in Fig. 11(b). We add MISRJ in the simulated echo, the input JSR is set as 30 dB, and the simulated SAR echoes and the jamming form are shown in Fig. 12. The proposed, adaptive filtering, and parameterized methods are used to suppress jamming. Then, the SAR imaging results using these three methods are shown in Fig. 13. We can see that the proposed method has much less residual jamming than the other two jamming suppression methods. The imaging result of the proposed method is closer to the imaging result without jamming.

(a) Simulated SAR imaging scene

(b) SAR imaging result without MISRJ

Fig. 11 SAR imaging scene

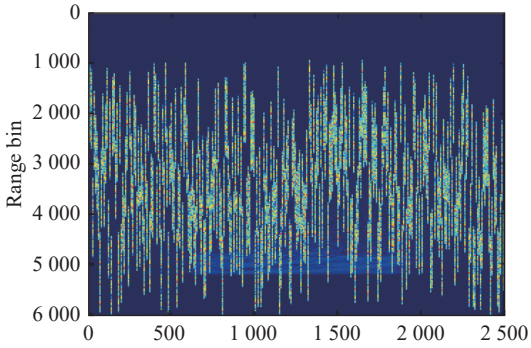

(a) SAR echoes with MISRJ

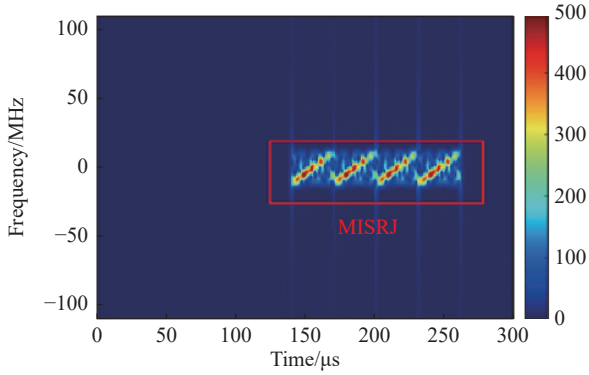

(b) Time-frequency distribution of echo

Fig. 12 Simulated echo with MISRJ

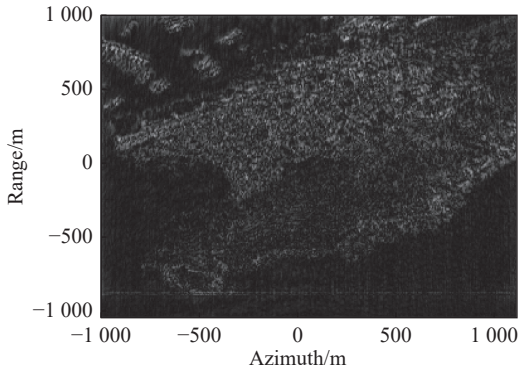

(a) SAR imaging result of adaptive filtering

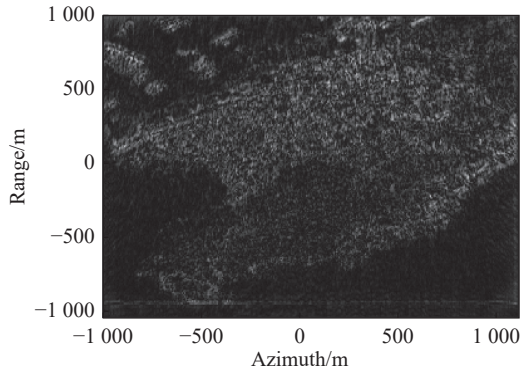

(b) SAR imaging result of the param eterized method

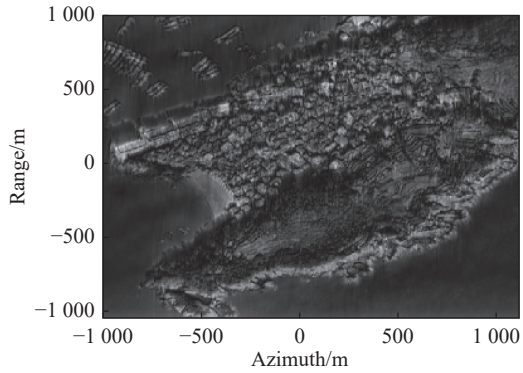

(c) SAR imaging result of the proposed method

Fig. 13 SAR imaging results with MISRJ

4.2 Real-measured data analysis

In order to verify the remarkable performance of the proposed method, the real-measured SAR data with MISRJ is used in this subsection. The SAR parameters are listed in Table 2, and the echo with jamming and its time-frequency distribution is shown in Fig. 14. The data is recorded using airborne SAR with Ka waveband and 1 GHz bandwidth. The spotlight model is utilized to observe a port. The distance between radar and scene is about 70 km and inertial navigation system (INS) is used to obtain the real-time position of platform. The data is recorded by the related research institution, and the research institution name and scene picture cannot be provided because of secrecy. From the SAR echo, we can see that MISRJ totally covers the real echoes of SAR, and the power of the MISRJ is more than 20 dB compared with real SAR echoes. The time-frequency distribution is also given in Fig. 14(b), and we can see that the MISRJ has complex modulation. The proposed, adaptive, and parameterized methods are used to suppress jamming and realize SAR imaging. The jamming suppression and SAR imaging results are shown in Fig. 15 and Fig. 16.

Table 2 Real-measured SAR parameters

Parameter	Value
f_c	Ka
B/MHz	100
T_p/μs	10
F_s/MHz	125
Pulse repetition frequency/Hz	600

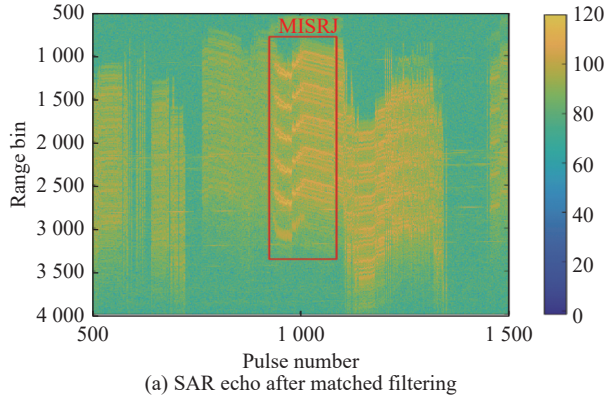

(a) SAR echo after matched filtering

(b) Time-frequency distribution of SAR echo with MISRJ

Fig. 14 Real-measured SAR echo with MISRJ

From Fig. 15(a), we can see that the real scene's time-frequency signals appear and the strong MISRJs are suppressed using the proposed method. However, the mass of residual jamming using the adaptive filtering method and parameterized method is shown in Fig. 15(b) and Fig. 15(c). Meanwhile, the scene signal has significant loss using adaptive filtering and parameterized methods. In addition, the SAR imaging results are also shown in Fig. 16, and we can see that the proposed jamming suppression method has the best imaging performance compared with the other two methods. The parameterized method cannot obtain SAR images because the complex modulation jamming mismatches with the parametrized jamming models. In this case, there is a mass of residual jamming in echoes leading to a lousy image result. In addition, compared with the adaptive filtering method, the SAR image using the proposed method has higher image SNR, better focusing performance, and clearer scene outline.

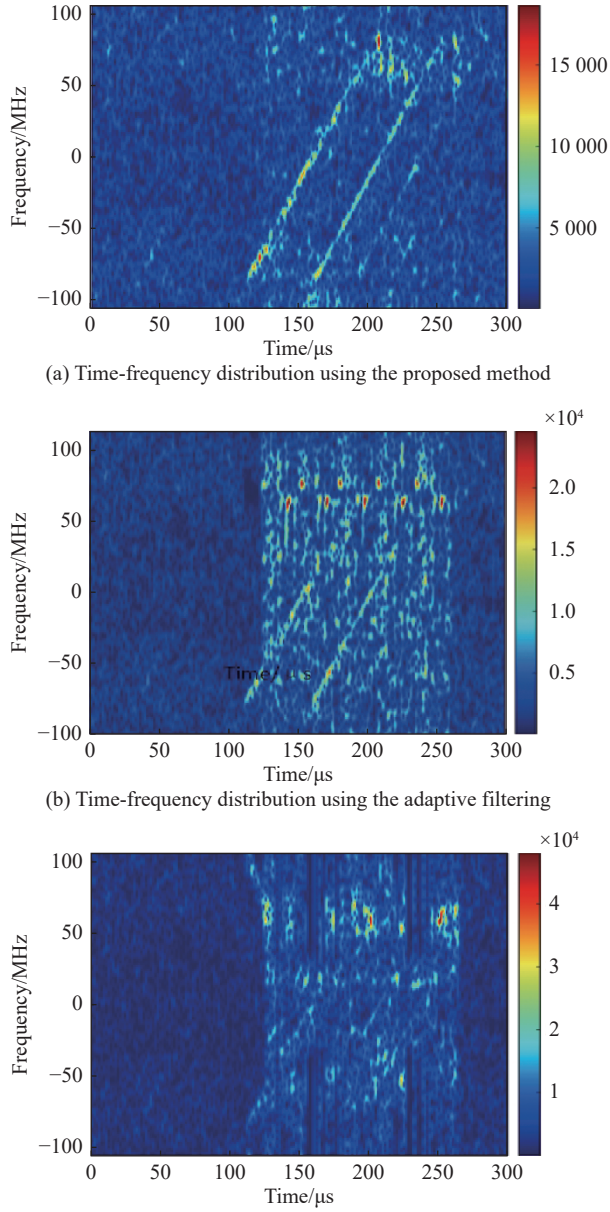

(a) Time-frequency distribution using the proposed method

(b) Time-frequency distribution using the adaptive filtering

(c) Time-frequency distribution using parametrized method

Fig. 15 Time-frequency distribution of echo with jamming suppression with different methods

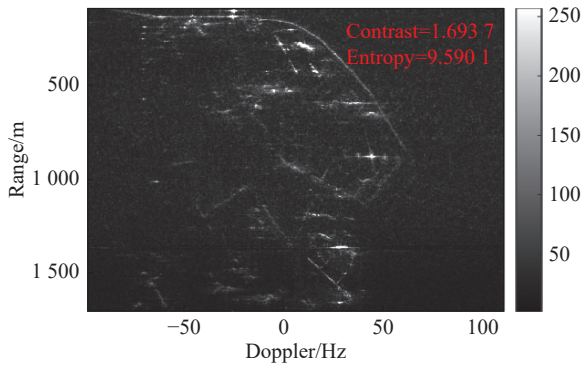

(a) SAR imaging using adaptive filtering method

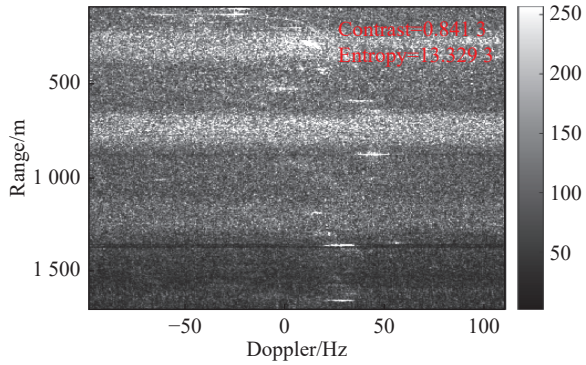

(b) SAR imaging using parameterized method

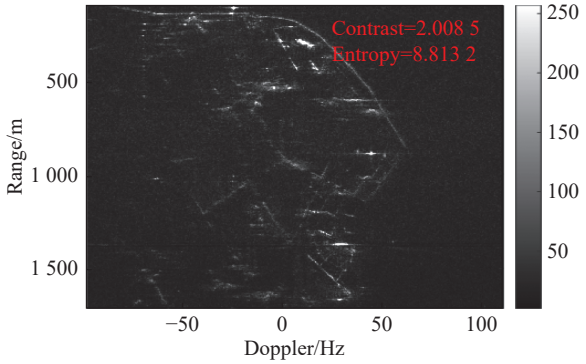

(c) SAR imaging using the proposed method

Fig. 16 SAR imaging results using different jamming suppression methods

In order to verify that the proposed method has better anti-jamming performance quantitatively, we also use the image entropy, contrast and signal to jamming and noise ratio (SJNR) to further evaluate the SAR images after anti-jamming. First, image contrast and entropy evaluate the image quality after anti-jamming. The definitions of entropy E and contrast C are

$$E = -\frac{1}{c}\sum_{r=1}^{R}\sum_{d=1}^{D}\left(\boldsymbol{I}(r,d) * \lg\left(\frac{\boldsymbol{I}(r,d)}{c}\right)\right), \tag{24}$$

$$C = \frac{\text{mean}(\boldsymbol{I})}{\text{var}(\boldsymbol{I})}, \tag{25}$$

where $\boldsymbol{I}(r,d)$ is the two-dimensional SAR image, c is a normalized constant, $\text{mean}(\cdot)$ is the image mean value, and $\text{var}(\cdot)$ is the variance of the image. As is known, the larger the contrast value and the smaller the entropy value, the higher quality of the SAR image. The image contrast and entropy of three images shown in Fig. 17 are listed in Table 3. We can see that the SAR image using the proposed method has the minimum image entropy and the maximum contrast compared with images using the other two methods. Thus it can be revealed that the proposed method's jamming suppress ability is the best.

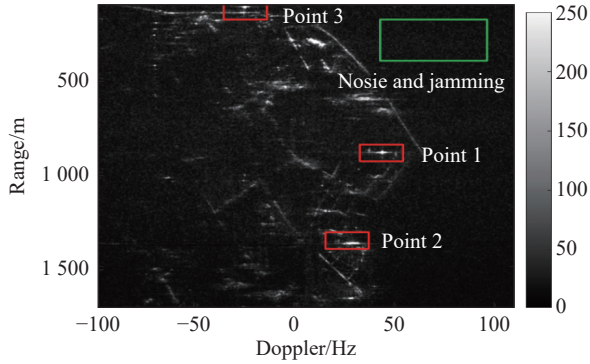

Fig. 17 Chosen scattering points for SJNR evaluation

Table 3 Image entropy and contrast after anti-jamming

Method	Entropy	Contrast
Method 1	8.813 2	2.008 5
Method 2	13.329 3	0.841 3
Method 3	9.590 1	1.693 7

In Table 3, Method 1 represents the proposed method, Method 2 represents the parameterized method, and Method 3 represents adaptive filtering method. Second, the SJNR of the strong scattering point in the SAR image after anti-jamming is calculated. It should be noticed that the higher SJNR reveals the better SAR image quality and the better anti-jamming quality. The SJNR of one scattering point in the SAR image is calculated as

$$\text{SJNR} = 10\lg\left(\frac{P_s}{P_{N/J}}\right) \tag{26}$$

where P_s is the power of scattering point and $P_{N/J}$ is the power of noise and rest jamming. We choose three strong scattering points P1, P2, and P3 to calculate SJNR, which are shown in Fig. 17. The SJNR of these three points are listed in Table 4. We can see that the SAR image using the proposed method has the highest SJNR in these three methods, which also reveals the best anti-jamming performance of the proposed method.

Table 4 SJNR of SAR images after anti-jamming dB

Method	P1	P2	P3
Method 1	53.015 1	45.726 6	39.430 5
Method 2	51.502 6	43.387 2	37.823 5
Method 3	17.829 7	14.126 2	19.294 3

In all, the real-measured imaging results reveal that the proposed method has better performance to suppress jamming and preserve real signals compared with the other two methods. The proposed method can be used in the practical jamming environment.

5. Conclusions

Combined with the MISRJ properties of large power, periodical transmitting and complex modulation, the proposed method has good performance to suppress MISRJ and persevere real radar signal at the same time. Due to extract jamming segments, the proposed method has high computational complexity. In this way, the anti-jamming method with low complexity should be further explored in our future works.

References

[1] LU J Y, ZHANG L, HUANG Y. High-resolution forward-looking multichannel SAR imagery with array deviation angle calibration. IEEE Trans. on Geoscience and Remote Sensing, 2020, 58(10): 6914–6928.

[2] LU J Y, ZHANG L, QUAN Y, et al. Parametric azimuth-variant motion compensation for forward-looking multichannel SAR imagery. IEEE Trans. on Geoscience and Remote Sensing, 2021, 59(10): 8521–8537.

[3] PERRY R P, DIPIETRO R C, FANTE R L. SAR imaging of moving targets. IEEE Trans. on Aerospace and Electronic Systems, 1999, 35(1): 188–200.

[4] SOLIMENE R, CATAPANO I, GENNARELLI G, et al. SAR imaging algorithms and some unconventional applications: a unified mathematical overview. IEEE Signal Processing Magazine, 2014, 31(4): 90–98.

[5] DONG X, ZHANG Y H. A novel compressive sensing algorithm for SAR imaging. IEEE Journal of Selected Topics in Applied Earth Observations and Remote Sensing, 2014, 7(2): 708–720.

[6] LIU Z D, ZHANG Q, LI G M, et al. Improved blanket jamming against ISAR based on nonperiodic interrupted sampling modulation. IEEE Sensors Journal, 2021, 21(1): 430–437.

[7] LI C Z, SU W M, GU H, et al. Improved interrupted sampling repeater jamming based on DRFM. Proc. of the IEEE International Conference on Signal Processing, Communications and Computing, 2014: 254–257.

[8] FENG D J, XU L T, PAN X Y, et al. Jamming wideband radar using interrupted-sampling repeater. IEEE Trans. on Aerospace and Electronic Systems, 2017, 53(3): 1341–1354.

[9] WU Q H, ZHAO F, AI X F, et al. Two-dimensional blanket jamming against ISAR using nonperiodic ISRJ. IEEE Sensors Journal, 2019, 19(11): 4031–4038.

[10] HUANG Q, XU Y M. Active cancellation stealth analysis based on interrupted-sampling and convolution modulation. Optic, 2016, 127(3): 3499–3503.

[11] DJUROVIC I, SIMEUNOVIC M, DJUROVIC S, et al. A hybrid CPF-HAF estimation of polynomial-phase signals: detailed statistical analysis. IEEE Trans. on Signal Processing, 2012, 10(60): 5010–5023.

[12] DJUKANOVIC S, POPOVIC V. A parametric method for multicomponent interference suppression in noise radars. IEEE Trans. on Aerospace and Electronic Systems, 2012, 48(3): 2730–2738.

[13] DJUKANOVIC S, DAKOVIC M, THAYAPARAN T. Method for non-stationary jammer suppression in noise radar systems. IET Signal Processing, 2010, 4(3): 305–313.

[14] STANKOVIC L, DJUKANOVIC S. Order adaptive local polynomial FT based interference rejection in spread spectrum communication systems. IEEE Trans. on Instrumentation and Measurement, 2005, 54(6): 2156–2162.

[15] ELGAMEL S A, SORAGHAN J, J. Using EMD-FrFT filtering to mitigate very high power interference in Chirp tracking radars. IEEE Signal Processing Letters, 2011, 18(4): 263–266.

[16] CHEN R, WANG Y M. Universal FRFT-based algorithm for parameter estimation of chirp signals. Journal of Systems Engineering and Electronics, 2012, 23(4): 495–501.

[17] LU Y L, LI M, CAO R Q, et al. Jointing time-frequency distribution and compressed sensing for countering smeared spectrum jamming. Journal of Electronics and Information Technology, 2016, 38(12): 3275–3281.

[18] XIE C X, ZHANG L M, ZHONG Z G. Quasi-LFM radar waveform recognition based on fractional Fourier transform and time-frequency analysis. Journal of Systems Engineering and Electronics, 2021, 32(5): 1130–1142.

[19] WEI D W, ZHANG S N, CHEN S, et al. Research on anti-jamming technology of chaotic composite short range detection system based on underdetermined signal separation and spectral analysis. IEEE Access, 2019, 7: 42298–42308.

[20] BARBAROSSA S, SCAGLIONE A. Adaptive time-varying cancellation of wideband interferences in spread-spectrum communications based on time-frequency distributions. IEEE Trans. on Signal Processing, 1999, 47(4): 957–965.

[21] CHIEN Y R. Design of GPS anti-jamming systems using adaptive notch filters. IEEE Systems Journal, 2015, 9(2): 451–460.

[22] LUO S C, XIONG Y, CHENG H, et al. An algorithm of radar deception jamming suppression based on blind signal separation. Proc. of the International Conference on Computational Problem-Solving, 2011: 167–170.

[23] HUANG G M, YANG L X, SU G Q. Blind source separation used for radar anti-jamming. Proc. of the International Conference on Neural Networks and Signal Processing, 2003, 2: 1382–1385.

[24] HUANG W Z, LIU Z, LV L T, et al. A novel anti-jamming driven sparse analysis-based spread spectrum communication methodology. International Journal of Pattern Recognition and Artificial Intelligence, 2019, 33(1): 1958001.

[25] HUANG Y, CHEN Z Y, WEN C, et al. Efficient radio frequency interference mitigation algorithm in real synthetic aperture radar data. IEEE Trans. on Geoscience and Remote Sensing, 2022, 60: 5224912.

[26] HUANG Y, WEN C, CHEN Z Y, et al. HRWS SAR narrowband interference mitigation using low-rank recovery and image-domain sparse regularization. IEEE Trans. on Geoscience and Remote Sensing, 2022, 60: 5217914.

[27] HUANG Y, ZHANG L, YANG X, et al. An efficient graph-based algorithm for time-varying narrowband interference suppression on SAR system. IEEE Trans. on Geoscience and Remote Sensing, 2021, 59(10): 8418–8432.

[28] HUANG Y, ZHANG L, LI J, et al. Reweighted tensor factorization method for SAR narrowband and wideband interference mitigation using smoothing multiview tensor model.

IEEE Trans. on Geoscience and Remote Sensing, 2022, 58(5): 3298–3313.
[29] ZHONG Y, LIU C L, ZHANG R. Research on narrowband anti-jamming technology based on compressed sensing. Proc. of the 12th International Symposium on Computational Intelligence and Design, 2019: 229–234.
[30] CHEN C, ZHUO Y N. A research on anti-jamming method based on compressive sensing for OFDM analogous system. Proc. of the IEEE 17th International Conference on Communication Technology, 2017: 655–659.
[31] LIU B Y, GUI G, MATSUSSHITA S Y, et al. Compressive sensing based direction-of-arrival estimation in MIMO radars in presence of strong jamming via blocking matrix. Proc. of the IEEE 10th Sensor Array and Multichannel Signal Processing Workshop, 2018: 292–296.
[32] HUANG Y, LIAO G S, XIANG Y, et al. Low-rank approximation via generalized reweighted iterative nuclear and Frobenius norms. IEEE Trans. on Image Processing, 2020, 29: 2244–2257.
[33] HUANG Y, LIAO G S, ZHANG L, et al. Efficient narrowband RFI mitigation algorithms for SAR systems with reweighted tensor structures. IEEE Trans. on Geoscience and Remote Sensing, 2019, 57(11): 9396–9409.
[34] HUANG Y, GUI S L, XIANG Y, et al. Reweighted nuclear norm and reweighted Frobenius norm minimizations for narrowband RFI suppression on SAR system. IEEE Trans. on Geoscience and Remote Sensing, 2019, 57(8): 5949–5962.
[35] HUANG Y, LIAO G S, ZHANG Z, et al. Fast narrowband RFI suppression algorithms for SAR systems via matrix-factorization techniques. IEEE Trans. on Geoscience and Remote Sensing, 2019, 57(1): 250–262.
[36] JULIEN M, BATCH F, PONCE J, et al. Online learning for matrix factorization and sparse coding. Journal of Machine Learning Research, 2010, 11(1): 19−60.
[37] LU C W, SHI J P, JIA J Y. Online robust dictionary learning. Proc. of the IEEE Conference on Computer Vision and Pattern Recognition, 2013: 415–422.
[38] GAO W, CHEN J, RICHARD C, et al. Online dictionary learning for kernel LMS. IEEE Trans. on Signal Processing, 2014, 62(11): 2765–2777.
[39] NADERAHAMADIAN Y S, BEHESHTI S, TINATI M A, et al. Correlation based online dictionary learning algorithm. IEEE Trans. on Signal Processing, 2015, 64(3): 592–602.

Biographies

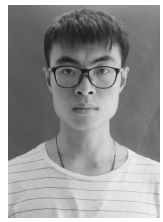

WEI Shaopeng was born in 1993. He received his B.S. degree in electronic engineering from Xidian University, Xi'an, China, in 2017, and Ph.D. degree in signal processing at the National Laboratory of Radar Signal Processing, Xidian University, in 2022. He is a lecturer in China University of Petroleum (East China). His rearch interests are radar signal processing and radar imaging.
E-mail: spwei@wpc.edu.cn

ZAHNG Lei was born in 1984. He received his Ph.D. degree in signal processing from Xidian University, Xi'an, China in 2012. From 2012 to 2019, he was an associate professor with the National Laboratory of Radar Signal Processing, Xidian University. He is working as a professor with the School of Electronics and Communication Engineering, Sun Yat-Sen University, Guangzhou, China. His major research interests are radar imaging synthetic aperture radar (SAR)/inverse SAR (ISAR) and motion compensation.
E-mail: zhanglei57@mail.sysu.edu.cn

LU Jingyue was born in 1994. He received his Ph.D. degree in signal processing from Xidian University, Xi'an, China, in 2021. He is currently a prospective associate professor with the School of Computer Science and Technology, Xidian University, Xi'an, China. His research interest is radar imaging.
E-mail: lujingyue@xidian.edu.cn

LIU Hongwei was born in 1971. He received his M.S. and Ph.D. degrees in electronic engineering from Xidian University, Xi'an, China, in 1995 and 1999, respectively. From 2001 to 2002, he was a visiting scholar with the Department of Electrical and Computer Engineering, Duke University, Durham, NC, USA. He works as a professor with the National Laboratory of Radar Signal Processing, Xidian University. His research interests include radar automatic target recognition, radar signal processing, and adaptive signal processing.
E-mail: hwliu@xidian.edu.cn